Phase behavior of a hard sphere Maier-Saupe nematogenic system in three dimensions

E. Lomba, C. Martín, and N. G. Almarza
Instituto de Química Física Rocasolano, CSIC, Serrano 119, E-28006 Madrid, Spain

F. Lado
Department of Physics, North Carolina State University, Raleigh, North Carolina 27695-8202, USA
(Received 27 April 2006; published 4 August 2006)

We present a detailed computer simulation and integral equation study of the phase behavior of a nematogenic system composed of hard spheres with embedded three-dimensional Maier-Saupe spins. For this well-known system, we map the gas-liquid equilibrium, which is coupled to a first-order isotropic-nematic transition. The anisotropic integral equation theory is found to yield excellent agreement with the simulation data within the fluid regime. Additionally, we determine the fluid-solid equilibrium transition by means of computer simulation.

DOI: 10.1103/PhysRevE.74.021503 PACS number(s): 64.70.Fx, 61.20.Gy, 64.60.Cn

I. INTRODUCTION

The phase behavior of systems composed of nonspherically symmetric particles, which undergo standard first-order gas-liquid and liquid-solid phase changes coupled to order-disorder transitions, continues to attract a great deal of interest. In these systems, the interplay between orientational and translational order (either local or long-range) plays the key role in modeling their phase diagrams. Among the simplest systems that are known to participate in this rich phenomenology are the ferromagnetic fluid models [1–14], in most cases composed of particles whose magnetic interaction is modeled via Heisenberg [1–3,7–9,11] or Ising [4,12,13] spins, embedded in either hard or soft spheres and with or without dispersive interactions. Recently, a three-dimensional *XY* spin system [14] has also been studied using an anisotropic integral equation approach. In all these cases, one typically encounters a second-order paramagnetic-ferromagnetic transition coupled with a gas-liquid equilibrium, with the second-order transition line meeting the gas-liquid equilibrium curve either at a tricritical point or at a critical endpoint, depending on the ratio between anisotropic and dispersive components of the interaction.

In addition to these magnetic models, another group of simple systems characterized by order-disorder transitions is composed of nematogenic fluids in which the orientational component of the interparticle interaction is essentially a Maier-Saupe term [15]. These systems exhibit isotropic-nematic transitions that might also be coupled to a gas-liquid transition if the range of attractive interactions is sufficiently large. The isotropic-nematic transition for Maier-Saupe particles with added dispersive interactions has been studied in some detail by means of computer simulation [16] and density functional theory [17]. In the latter case, a full picture of the phase diagram was obtained indicating that, when dealing with Maier-Saupe interactions coupled with dispersive forces, one finds a continuous change from a first-order gas-liquid transition to a first-order isotropic-nematic transition. Recently, the present authors [18,19] examined a simple model of Maier-Saupe fluid in which the decay of the anisotropic interaction is determined by a Yukawa functional form with no attractive component in the interparticle potential and having the peculiarity that the three-dimensional spins are embedded in hard spheres whose centers are constrained to lie in a plane. This model, which is a continuum version of the RP^2 model [20], was found to undergo a Berezinskii-Kosterliz-Thouless (BKT) continuous order-disorder transition [21] coupled to a condensation transition at low temperatures in which the ordered phase lacks a true long-range order.

A simpler natural extension of the BKT work of Ref. [21] is the study of a Maier-Saupe hard sphere fluid in three dimensions, the model we take up here. From the studies performed in Refs. [16,17], one should expect the BKT order-disorder transition in this case to shift into a first-order transition, the nematic order now being truly long ranged. According to the anisotropic mean spherical approximation calculations of Sokolovska *et al.* [22] for this model, a first-order isotropic-nematic transition is to be found in the liquid regime, although these authors do not present results for the complete phase diagram. In fact, aside from the density functional theory calculations of Ref. [17], we are not aware of any work in which the complete phase diagram for Maier-Saupe fluids without dispersive interactions has been determined.

In this paper, then, we focus on the phase behavior of a simple three-dimensional hard sphere Maier-Saupe fluid, which is, so to speak, the unconstrained version of the planar model previously studied by us [18,19]. The potential energy of this system is prescribed by

$$U = \sum_j u_z(\omega_j) + \sum_{i<j} u_{\mathrm{HS}}(r_{ij}) + \sum_{i<j} u(r_{ij}, \omega_i, \omega_j), \qquad (1)$$

where $\omega = (\theta, \phi)$ specifies the orientation of a molecular nematic axis. Here the one-body interaction

$$u_z(\omega) = -W_0 P_2(\cos\theta), \quad \text{with } W_0 \geq 0, \qquad (2)$$

arises from an external field which defines the z axis. To this one adds the hard sphere pair potential, $u_{\mathrm{HS}}(r)$, for spheres of diameter σ and an orientation-dependent potential between a pair of molecules that tends to align their mutual nematic axes,

$$u(r,\omega_1,\omega_2) = -Ku_0(r)P_2(\cos\theta_{12}), \quad \text{with } K>0, \tag{3}$$

where

$$u_0(r) = \frac{e^{-\kappa(r/\sigma-1)}}{r/\sigma} - \frac{e^{-\kappa(R/\sigma-1)}}{R/\sigma}, \quad \sigma \le r \le R, = 0, \quad r > R. \tag{4}$$

Here, $P_2(x)=(3x^2-1)/2$ is the Legendre polynomial of order 2, θ_{12} is the angle between the axes of molecules 1 and 2, κ is a dimensionless range parameter, and K determines the strength of the coupling interaction. The potential $u_0(r)$ is truncated and shifted at $R=4\sigma$ for computational convenience in the simulation. In the calculations, we define the reduced temperature as $T^*=k_BT/K=(\beta K)^{-1}$ and the reduced external field as $W_0^*=W_0/K$, where T is the absolute temperature and k_B is Boltzmann's constant. We have set the range parameter at $\kappa=1$.

As the main tools of our study, we use extensive *NVT* and *NpT* Monte Carlo simulations in conjunction with the anisotropic Ornstein-Zernike integral equation, the latter in a manner that has been successfully exploited to describe Heisenberg spin fluids [8,9]. We determine in this way the complete phase diagram of our model, which is shown to exhibit an isotropic-nematic transition that is weakly first order at high temperatures and couples smoothly to a gas-liquid transition as the temperature is lowered. We find that the net attraction produced by the anisotropic interaction is sufficiently long ranged to induce the condensation of the liquid. Finally, for the sake of completeness, we also determine the fluid-(fcc)solid equilibria.

The remainder of the paper is organized as follows. In the next section we summarize key aspects of the integral equation calculations, while specific details of the calculation of phase equilibria using computer simulation are presented in Sec. III. Finally, in Sec. IV we discuss our most significant results.

II. THE ANISOTROPIC ORNSTEIN-ZERNIKE EQUATION

Integral equations provide a computationally efficient route to the thermodynamics of the Maier-Saupe fluid in an external field, at the cost of an approximation [23,24]. For example, once the one-body distribution function, $f(\omega)$, and the two-body distribution function, $g(r,\omega_1,\omega_2)$, have been determined the internal energy U and pressure p are given by quadratures

$$\frac{\beta U}{N} = -\beta W_0\langle P_2(\cos\theta)\rangle + \frac{1}{2}\frac{\rho}{(4\pi)^2}\int d\mathbf{r}\, d\omega_1 d\omega_2 \times f(\omega_1)f(\omega_2)g(r,\omega_1,\omega_2)\beta u(r,\omega_1,\omega_2), \tag{5}$$

$$\frac{\beta p}{\rho} = 1 - \frac{1}{6}\frac{\rho}{(4\pi)^2}\int d\mathbf{r}\, d\omega_1 d\omega_2 f(\omega_1)f(\omega_2) \times g(r,\omega_1,\omega_2) r\frac{d}{dr}[\beta u_{\mathrm{HS}}(r) + \beta u(r,\omega_1,\omega_2)]. \tag{6}$$

Other quadratures yield the magnetic susceptibilities, Helmholtz free energy, and chemical potential used in the sequel. The goal then is to find $f(\omega)$ and $g(r,\omega_1,\omega_2)$.

A. Tailored Legendre functions

We note first that pair functions such as $g(r,\omega_1,\omega_2)=g(r,\theta_1,\theta_2,\phi_1-\phi_2)$ depend on four independent variables, so that as a practical matter an expansion in some orthogonal basis set is needed to make them computationally tractable. For molecular fluids, this normally means the spherical harmonics

$$Y_{lm}(\omega) = \frac{(-1)^m}{\sqrt{4\pi}} e^{im\phi}\hat{P}_{lm}(\cos\theta), \tag{7}$$

where the $\hat{P}_{lm}(\cos\theta)$ are the familiar Legendre functions, but here normalized so that

$$\frac{1}{2}\int_{-1}^{1} d(\cos\theta)\hat{P}_{lm}(\cos\theta)\hat{P}_{l'm}(\cos\theta) = \delta_{ll'}. \tag{8}$$

Under the anisotropic conditions created by the external field, however, the orthogonality of Eq. (8) is no longer useful, since now the molecular orientation angle θ is nonuniformly distributed according to some distribution $f(\omega)=f(\cos\theta)$. Thus we introduce new, *tailored* Legendre functions $\mathcal{P}_{lm}(\cos\theta)$ that are explicitly constructed to be orthogonal with weight function $f(\cos\theta)$,

$$\frac{1}{2}\int_{-1}^{1} d(\cos\theta)f(\cos\theta)\mathcal{P}_{lm}(\cos\theta)\mathcal{P}_{l'm}(\cos\theta) = \delta_{ll'}. \tag{9}$$

Now with the corresponding generalized spherical harmonics

$$\mathcal{Y}_{lm}(\omega) = \frac{(-1)^m}{\sqrt{4\pi}} e^{im\phi}\mathcal{P}_{lm}(\cos\theta), \tag{10}$$

we can expand pair functions such as $g(r,\omega_1,\omega_2)$ in the form ($\bar{m}\equiv -m$)

$$g(r,\omega_1,\omega_2) = 4\pi\sum_{l_1,l_2,m} g_{l_1l_2m}(r)\mathcal{Y}_{l_1m}(\omega_1)\mathcal{Y}_{l_2\bar{m}}(\omega_2). \tag{11}$$

In this work, the generalized spherical harmonics (10) follow the Condon-Shortley phase convention [25]. Construction of the generalized Legendre functions $\mathcal{P}_{lm}(\cos\theta)$ is described in Ref. [9].

B. Ornstein-Zernike equation and closure

Pair functions such as $g(r,\omega_1,\omega_2)\equiv 1+h(r,\omega_1,\omega_2)$ are obtained as numerical solutions of two coupled nonlinear equations: the anisotropic Ornstein-Zernike equation and a closure equation [23,24]. Using the generalized spherical harmonics, one quickly reduces the anisotropic Ornstein-Zernike equation to a sequence of matrix equations for coefficients [9],

$$\tilde{\mathbf{\Gamma}}_m(k) = (-1)^m\rho\tilde{\mathbf{C}}_m(k)\tilde{\mathbf{C}}_m(k)[\mathbf{I}-(-1)^m\rho\tilde{\mathbf{C}}_m(k)]^{-1}, \tag{12}$$

where $\tilde{\mathbf{\Gamma}}_m(k)$ and $\tilde{\mathbf{C}}_m(k)$ are symmetric matrices with elements, respectively, $\tilde{\gamma}_{l_1l_2m}(k)$ and $\tilde{c}_{l_1l_2m}(k)$, for

$l_1, l_2 \geq m = 0, 1, 2, \ldots$, and $\mathbf{I}$ is the unit matrix. The most notable feature of Eq. (12) is that it is *identical* to that of an isotropic system with no external field. All of the anisotropy is built into the basis functions.

In Eq. (12) we have introduced Fourier transforms of the direct correlation function $c(r, \omega_1, \omega_2)$ and the indirect correlation function $\gamma(r, \omega_1, \omega_2) = h(r, \omega_1, \omega_2) - c(r, \omega_1, \omega_2)$. Because the orientations of spins 1 and 2 and that of $\mathbf{r}_{12}$ are decoupled in the Maier-Saupe model, the Fourier transforms may be performed holding the former fixed. A transform pair is then

$$\tilde{\gamma}(k, \omega_1, \omega_2) = 4\pi \int_0^\infty dr\, r^2 \gamma(r, \omega_1, \omega_2) \frac{\sin(kr)}{kr}, \quad (13)$$

$$\gamma(r, \omega_1, \omega_2) = \frac{1}{2\pi^2} \int_0^\infty dk\, k^2 \tilde{\gamma}(k, \omega_1, \omega_2) \frac{\sin(kr)}{kr}, \quad (14)$$

and the transformed functions may themselves be expanded,

$$\tilde{\gamma}(k, \omega_1, \omega_2) = 4\pi \sum_{l_1, l_2, m} \tilde{\gamma}_{l_1 l_2 m}(k) \mathcal{Y}_{l_1 m}(\omega_1) \mathcal{Y}_{l_2 \bar{m}}(\omega_2), \quad (15)$$

with expansion coefficients $\tilde{\gamma}_{l_1 l_2 m}(k)$ that are individually the transforms of $\gamma_{l_1 l_2 m}(r)$.

The second, or closure, equation [23,24] is

$$c(r, \omega_1, \omega_2) = \exp[-\beta u_{\mathrm{HS}}(r) - \beta u(r, \omega_1, \omega_2) + \gamma(r, \omega_1, \omega_2) + b(r, \omega_1, \omega_2)] - 1 - \gamma(r, \omega_1, \omega_2). \quad (16)$$

This relation must be supplemented with an approximation for b, the so-called bridge function, which is formally defined in terms of a diagram summation [23] that offers little practical benefit. In this work, we have used the reference hypernetted-chain (RHNC) equation [26], which consists in approximating b with the known bridge function b^{Ref} of some reference system. If the Helmholtz free energy is also sought within the RHNC scheme, as is the case here, then in practice only a hard sphere reference is currently well enough known for this substitution, so we put

$$b(r, \omega_1, \omega_2) \approx b_{\mathrm{HS}}(r; \sigma_{\mathrm{Ref}}), \quad (17)$$

where σ_{Ref} is the reference sphere diameter that may be varied [27] to attain a minimized free energy [28]. For the modeled hard sphere functions we use the parametrizations of Verlet-Weis [29] and Henderson-Grundke [30].

C. Equations for $f(\cos\theta)$

The unperturbed one-body distribution function is given by $\ln f_0(\cos\theta) = \mathrm{const} + \beta W_0 P_2(\cos\theta)$, where const is determined by the normalization

$$\frac{1}{2} \int_{-1}^{1} d(\cos\theta) f_0(\cos\theta) = 1. \quad (18)$$

We find then

$$f_0(\cos\theta) = \frac{\sqrt{\frac{3}{2}\beta W_0}}{D\left(\sqrt{\frac{3}{2}\beta W_0}\right)} \exp\left[\tfrac{3}{2}\beta W_0 (\cos^2\theta - 1)\right], \quad (19)$$

where $D(x)$ is Dawson's integral,

$$D(x) \equiv e^{-x^2} \int_0^x e^{s^2} ds. \quad (20)$$

There are now two exact equations that can be used to find $f(\cos\theta)$ for an *interacting* system: the Triezenberg-Zwanzig-Lovett-Mou-Buff-Wertheim (TZLMBW) equation [31] and the first member of the Kirkwood-Yvon-Born-Green (KYBG) equation [23].

The TZLMBW equation reads

$$\hat{\boldsymbol{\varphi}}_1 \frac{d}{d\theta_1} \ln\left[\frac{f(\cos\theta_1)}{f_0(\cos\theta_1)}\right] = \frac{\rho}{4\pi} \int d\mathbf{r}\, d\omega_2 f(\cos\theta_2) \times c(r, \omega_1, \omega_2) \hat{\boldsymbol{\varphi}}_2 \frac{d \ln f(\cos\theta_2)}{d\theta_2}; \quad (21)$$

where $\hat{\boldsymbol{\varphi}}_i$ is the azimuthal unit vector. Dotting $\hat{\boldsymbol{\varphi}}_1$ into (21) converts it into a scalar equation. If we now put

$$\ln f(\cos\theta) = \sum_{l=0}^{\infty} A_l \mathcal{P}_{l0}(\cos\theta) \quad (22)$$

and expand $c(r, \omega_1, \omega_2)$ as in Eq. (11), we get first

$$\sum_l A_l \frac{d\mathcal{P}_{l0}(\cos\theta)}{d\theta} = -3\beta W_0 \sin\theta \cos\theta + \sum_{l_1, l_2, l_3} \mathcal{P}_{l_1 1}(\cos\theta) \rho \tilde{c}_{l_1 l_2 1}(0) B_{l_2 l_3} A_{l_3}, \quad (23)$$

where

$$B_{l_1 l_2} \equiv -\frac{1}{2} \int_{-1}^{1} d(\cos\theta) f(\cos\theta) \mathcal{P}_{l_1 1}(\cos\theta) \frac{d\mathcal{P}_{l_2 0}(\cos\theta)}{d\theta}. \quad (24)$$

It follows then from Eq. (23) that

$$\sum_{l_3} B_{l_1 l_3} A_{l_3} = 3\beta W_0 (m_2 - m_4)^{1/2} \delta_{l_1 2} - \sum_{l_2, l_3} \rho \tilde{c}_{l_1 l_2 1}(0) B_{l_2 l_3} A_{l_3}, \quad (25)$$

or, in matrix notation,

$$[\mathbf{I} + \rho \tilde{\mathbf{C}}_1(0)] \mathbf{B} \mathbf{a} = 3\beta W_0 (m_2 - m_4)^{1/2} \mathbf{u}_2. \quad (26)$$

Here $\mathbf{B}$ is a bidiagonal matrix with nonzero elements B_{ll} and $B_{l,l+2}$ $(l \geq 1)$, while $\mathbf{a}$ and $\mathbf{u}_2$ are column matrices with elements $(A_1, A_2, A_3, A_4, \ldots)$ and $(0, 1, 0, 0, \ldots)$, respectively. We have finally from (26),

$$A_l = 3\beta W_0 (m_2 - m_4)^{1/2} Q_{l2}, \quad (27)$$

where $\mathbf{Q} \equiv \mathbf{B}^{-1} [\mathbf{I} + \rho \tilde{\mathbf{C}}_1(0)]^{-1}$.

The A_l coefficients vanish for l odd. It will also turn out that A_2 is larger than A_4 by at least two orders of magnitude, so that we may ignore A_4 and higher coefficients in the analysis above to get the simpler form

$$A_2 \approx \frac{3\beta W_0(m_2-m_4)^{1/2}}{B_{22}[1+\rho\tilde{c}_{221}(0)]},$$

$$\approx \frac{3}{2}\beta W_0 \frac{(m_4-m_2^2)^{1/2}}{1+\rho\tilde{c}_{221}(0)}, \tag{28}$$

where we have used $B_{22}=2[(m_2-m_4)/(m_4-m_2^2)]^{1/2}$. Then the *form* of the angular distribution function remains unchanged from the original unperturbed case,

$$\ln f(\cos\theta) \approx \text{const} + \beta W P_2(\cos\theta), \tag{29}$$

but the *effective* field in the interacting system is now

$$W = \frac{W_0}{1+\rho\tilde{c}_{221}(0)}. \tag{30}$$

We find by calculation that Eq. (29) is essentially exact in the context of the numerical solution.

In the equations above we have used some moments of the one-body distribution function,

$$m_k \equiv \frac{1}{2}\int_{-1}^{1} dx\, f(x)x^k, \tag{31}$$

and the specific generalized functions

$$\mathcal{P}_{20}(\cos\theta) = \frac{\cos^2\theta - m_2}{(m_4-m_2^2)^{1/2}}, \tag{32}$$

$$\mathcal{P}_{21}(\cos\theta) = \frac{\sin\theta\cos\theta}{(m_2-m_4)^{1/2}}. \tag{33}$$

Calculation of $f(\cos\theta)$ from the KYBG equation follows closely the analysis in Ref. [18] and requires no further elaboration here.

D. Thermodynamics

With expansions in the tailored orthogonal basis, the fourfold integrals in Eqs. (5) and (6) immediately reduce in each case to a final quadrature,

$$\frac{\beta U}{N} = -\beta W_0\langle P_2(\cos\theta)\rangle + \frac{1}{2}\rho\sum_{l_1,l_2,m}\int_\sigma^\infty g_{l_1l_2m}(r)\beta u_{l_1l_2m}(r)4\pi r^2 dr, \tag{34}$$

$$\frac{\beta p}{\rho} = 1 + \frac{2}{3}\pi\rho\sigma^3 g_{000}(\sigma) - \frac{1}{6}\rho\sum_{l_1,l_2,m}\int_\sigma^\infty g_{l_1l_2m}(r) r\frac{d\beta u_{l_1l_2m}(r)}{dr}4\pi r^2 dr, \tag{35}$$

that is evaluated numerically with the trapezoidal rule. The coefficients of the potential $u(r,\omega_1,\omega_2)$ are $u_{l_1l_2m}(r)=-Ku_0(r)P_{l_1l_2m}$, with nonzero elements [18]

$$P_{000} = \tfrac{1}{4}(3m_2-1)^2, \tag{36}$$

$$P_{200} = P_{020} = \tfrac{3}{4}(3m_2-1)(m_4-m_2^2)^{1/2}, \tag{37}$$

$$P_{220} = \tfrac{9}{4}(m_4-m_2^2), \tag{38}$$

$$P_{221} = P_{22-1} = -\tfrac{3}{2}(m_2-m_4), \tag{39}$$

$$P_{222} = P_{22-2} = \tfrac{3}{8}(1-2m_2+m_4). \tag{40}$$

Turning off the pair interactions, we readily find for the ideal Helmholtz free energy

$$\frac{\beta F^{\text{id}}}{N} = \ln(\rho\Lambda^3) - 1 - \ln\left[\frac{e^{\beta W_0}D\left(\sqrt{\tfrac{3}{2}\beta W_0}\right)}{\sqrt{\tfrac{3}{2}\beta W_0}}\right], \tag{41}$$

where Λ is the thermal de Broglie wavelength. Then following the analysis of Ref. [9] we get for the excess free energy, $F^{\text{ex}} \equiv F - F^{\text{id}}$,

$$\frac{\beta F^{\text{ex}}}{N} = \left\langle \ln\left[\frac{f(\cos\theta)}{f_0(\cos\theta)}\right]\right\rangle + \frac{\beta F_1}{N} + \frac{\beta F_2}{N} + \frac{\beta F_3}{N}, \tag{42}$$

with

$$\frac{\beta F_1}{N} = -\frac{1}{2}\rho\int d\mathbf{r}\left\{c_{000}(r) + \frac{1}{2}\sum_{l_1,l_2,m}[c^2_{l_1l_2m}(r) - \gamma^2_{l_1l_2m}(r)]\right\}, \tag{43}$$

$$\frac{\beta F_2}{N} = -\frac{1}{2\rho}\int\frac{d\mathbf{k}}{(2\pi)^3}\sum_m \{\ln\det[\mathbf{I} + (-1)^m\rho\tilde{\mathbf{H}}_m(k)] - (-1)^m\text{tr}[\rho\tilde{\mathbf{H}}_m(k)]\}, \tag{44}$$

$$\frac{\beta F_3}{N} = \frac{1}{2}\rho\int d\mathbf{r}\int_0^1 d\lambda\sum_{l_1,l_2,m} g_{l_1l_2m}(r|\lambda)\frac{\partial b_{l_1l_2m}(r|\lambda)}{\partial\lambda}. \tag{45}$$

The final integral over the "charging" parameter λ in Eq. (45) cannot be evaluated in closed form and this term must be approximated. In the hypernetted-chain closure [32], it is simply neglected.

The effect of the RHNC approximation is to replace Eq. (45) with the corresponding integral of the reference system, which is then evaluated as $F_3^{\text{Ref}}=F^{\text{Ref}}-F_1^{\text{Ref}}-F_2^{\text{Ref}}$. With the hard sphere system as a reference, we have then

$$\frac{\beta F^{\text{ex}}_{\text{RHNC}}}{N} = \frac{\beta F^{\text{ex}}_{\text{HS}}}{N} + \left\langle \ln\left[\frac{f(\cos\theta)}{f_0(\cos\theta)}\right]\right\rangle + \frac{\beta\Delta F_1}{N} + \frac{\beta\Delta F_2}{N}, \tag{46}$$

where $\Delta F_k = F_k - F_k^{\text{HS}}$.

Finally, the chemical potential μ is found as $\beta\mu = \beta F/N + \beta p/\rho$.

E. Susceptibilities

To generate expressions for the susceptibility of our nematogenic system, we temporarily introduce an external vector field $\mathbf{H}$ such that $W_0=H^2$ and

$$W_0 P_2(\cos\theta) = \tfrac{1}{2}[3(\hat{\mathbf{s}}\cdot\mathbf{H})^2 - H^2], \tag{47}$$

where $\hat{\mathbf{s}}$ is a unit vector in the direction of the nematic axis.

The "magnetization" in the direction $\alpha=x,y,z$ is then

$$M_\alpha = \frac{1}{\beta}\frac{\partial \ln Z}{\partial H_\alpha} = \left\langle \sum_j [3(\hat{\mathbf{s}}_j\cdot\mathbf{H})s_{j\alpha} - H_\alpha] \right\rangle, \tag{48}$$

where Z is the canonical partition function, while the susceptibility tensor is

$$\chi_{\alpha\beta} \equiv \frac{1}{V}\frac{\partial M_\alpha}{\partial H_\beta} = \frac{\beta}{V}\left\langle \sum_i [3(\hat{\mathbf{s}}_i\cdot\mathbf{H})s_{i\alpha} - H_\alpha]\sum_j [3(\hat{\mathbf{s}}_j\cdot\mathbf{H})s_{j\beta} - H_\beta] \right\rangle - \frac{\beta}{V}\left\langle \sum_i [3(\hat{\mathbf{s}}_i\cdot\mathbf{H})s_{i\alpha} - H_\alpha] \right\rangle \left\langle \sum_j [3(\hat{\mathbf{s}}_j\cdot\mathbf{H})s_{j\beta} - H_\beta] \right\rangle + \frac{1}{V}\left\langle \sum_j (3s_{j\alpha}s_{j\beta} - \delta_{\alpha\beta}) \right\rangle. \tag{49}$$

Now set $\mathbf{H}$ along the z axis, so that $H_x=H_y=0$, $H_z=H$, and $s_x=\sin\theta\cos\phi$, $s_y=\sin\theta\sin\phi$, and $s_z=\cos\theta$. Then we get finally $M_x=M_y=0$ and $M_z=M$, with

$$M = 2N\langle P_2(\cos\theta)\rangle H, \tag{50}$$

while the transverse and longitudinal susceptibilities are $\chi_T \equiv \frac{1}{2}(\chi_{xx}+\chi_{yy})$ and $\chi_L \equiv \chi_{zz}$, respectively. These yield contributions from both one-body and two-body terms:

$$\chi_T = \chi_T^{(1)} + \chi_T^{(2)}, \tag{51}$$

$$\chi_T^{(1)}/\rho = -\langle P_2(\cos\theta)\rangle, \tag{52}$$

$$\chi_T^{(2)}/\rho\beta W_0 = \tfrac{9}{2}(m_2 - m_4)[1 - \rho\tilde{h}_{221}(0)], \tag{53}$$

for the transverse susceptibility, and

$$\chi_L = \chi_L^{(1)} + \chi_L^{(2)}, \tag{54}$$

$$\chi_L^{(1)}/\rho = 2\langle P_2(\cos\theta)\rangle, \tag{55}$$

$$\chi_L^{(2)}/\rho\beta W_0 = (3m_2 - 1)^2[1 + \rho\tilde{h}_{000}(0)] + 6(3m_2 - 1)(m_4 - m_2^2)^{1/2}\rho\tilde{h}_{200}(0) + 9(m_4 - m_2^2)[1 + \rho\tilde{h}_{220}(0)], \tag{56}$$

for the longitudinal susceptibility. The off-diagonal elements of $\boldsymbol{\chi}$ are zero.

III. SIMULATION METHODS FOR PHASE EQUILIBRIA CALCULATIONS

The first problem one encounters when simulating a system near critical conditions is the presence of large scale fluctuations and critical slowing down. In this work we employ the same efficient cluster algorithms [33] used in Refs. [2,19] combined with the local update algorithm and histogram reweighting techniques [34] used in Ref. [19].

In order to compute the phase equilibria of our system we have used different procedures. For the calculation of the liquid-vapor equilibrium (i.e., fluid-fluid equilibrium at low temperatures) and the fluid-solid coexistence we make use of thermodynamic integration methods, while for the fluid-fluid equilibrium at high temperatures we perform a finite-size scaling analysis of a series of NpT simulations.

A. Thermodynamic integration techniques

The free energy of the gas phase for a given temperature can be determined by carrying out NVT simulations at several low densities and fitting the pressure results to a virial equation of state,

$$\beta p(\rho,\beta) = \rho + \sum_{k\geq 2} B_k \rho^k. \tag{57}$$

With the equation of state of the gas in hand, we can then compute the Helmholtz free energy F as

$$\frac{\beta F(\rho,\beta)}{N} = \frac{\beta F_0(\beta)}{N} + \ln(\rho\Lambda^3) - 1 + \int_0^\rho d\xi \frac{\beta p(\xi,\beta) - \xi}{\xi^2}, \tag{58}$$

where F_0, the kinetic contribution to the free energy, does not depend on the density [see Eq. (41)]. The free energy of the high density phases (which exhibit nematic order) can be evaluated using thermodynamic integration. In this case we choose as a reference state a hard sphere fluid (or solid) at a given density. We then perform thermodynamic integration up to a corresponding hard sphere Yukawa system at a certain temperature. The free energy of the latter can easily be connected to that of our Maier-Saupe fluid (or solid) when both systems are under the influence of an external field. Later on, one switches off the external field and the plain Maier-Saupe system is recovered. The method we have followed is similar to that used in Ref. [10] and is implemented as follows. One first considers two related models: the Maier-Saupe (MS) system, as described above, and a Yukawa (Y) model which lacks spin-spin interactions, so that the interparticle potential reduces to

$$u_Y(r,\omega_1,\omega_2) = -Ku_0(r), \quad \text{with } K>0. \tag{59}$$

Note that the noninteracting spins still do couple with the external field. Maier-Saupe and Yukawa models are equivalent in the limit of very intense external fields ($W_0\to\infty$). One can, therefore, compute the free energy difference between the models at *zero* external field using

$$F_{MS} = F_Y - \int_0^\infty dW_0 \left[\frac{\partial F_{MSF}}{\partial W_0} - \frac{\partial F_{YF}}{\partial W_0}\right], \tag{60}$$

or

$$\frac{F_{\mathrm{MS}}}{N} = \frac{F_{\mathrm{Y}}}{N} + \int_0^\infty dW_0[\bar{P}_2^{\mathrm{MSF}}(W_0) - \bar{P}_2^{\mathrm{YF}}(W_0)], \tag{61}$$

where MSF and YF refer, respectively, to the Maier-Saupe and Yukawa models with an external field and

$$\bar{P}_2(W_0) \equiv \frac{1}{N}\left\langle \sum_{j=1}^{N} P_2(\cos\,\theta_j) \right\rangle = -\frac{1}{N}\frac{\partial F}{\partial W_0}. \tag{62}$$

In the YF model the interparticle interactions do not depend on the orientation of the nematic axis, so $\bar{P}_2^{\mathrm{YF}}(W_0)$ can be directly evaluated as

$$\bar{P}_2^{\mathrm{YF}}(W_0) = \frac{\int_{-1}^{1} dx\, e^{\beta W_0 P_2(x)} P_2(x)}{\int_{-1}^{1} dx\, e^{\beta W_0 P_2(x)}}. \tag{63}$$

In order to minimize numerical inaccuracies in the evaluation of (61), it is convenient to replace the integration variable W_0 by

$$\omega = \frac{W_0}{W_m + W_0}, \tag{64}$$

with W_m a const; we then have

$$\frac{F_{\mathrm{MS}}}{N} = \frac{F_{\mathrm{Y}}}{N} + W_m \int_0^1 d\omega \frac{\bar{P}_2^{\mathrm{MSF}}(\omega) - \bar{P}_2^{\mathrm{YF}}(\omega)}{(1-\omega)^2}. \tag{65}$$

With an appropriate choice of W_m we can get a smooth integrand in (65).

To study the liquid-vapor equilibrium of the system, we evaluate the free energy of the Yukawa model for two systems, with a number of particles $N=500$, density $\rho\sigma^3=0.80$, and temperatures $T^*=2.0$ and $T^*=3.0$, using the standard thermodynamic integration from the hard sphere system [10]. We then compute the free energy of the MS model in the same thermodynamic states using the thermodynamic integration route as given in Eq. (65) and perform around 20 simulations of the MSF model at each temperature for different values of the parameter ω. Finally, we carry out a number of *NVT* simulations of the zero-field Maier-Saupe system at the same density and different temperatures to produce the corresponding reference data to study the liquid-vapor equilibrium along various isotherms. The use of two temperatures lets us check the consistency of the procedure.

1. Liquid-vapor equilibrium

We have performed *NVT* Monte Carlo simulations along selected isotherms, fitting the low density results to Eq. (57). The pressures at high density are fitted to a second-order polynomial. With the corresponding equations of state and the respective reference states at low and high densities, we can then compute both the pressure and the chemical potential as functions of the density and locate the phase equilibrium conditions.

2. Liquid-solid equilibrium

We have assumed a face-centered-cubic (fcc) structure of the solid near melting. In fact, the hexagonal close packing could actually be the more stable phase. At a constant density, the potential energy of the hexagonal close-packing structure is somewhat lower than that of the fcc structure. Nevertheless, the differences in free energy between the two close-packing structures are expected to be so small that the overall solid-liquid diagram should hardly be affected. We have again performed a thermodynamic integration from the hard sphere fluid and solid phases, following the strategy sketched above. Because of the potential range of the model, we chose systems with $N=864$. The reference densities were chosen to be $\rho\sigma^3=0.80$ for the fluid and $\rho\sigma^3=1.05$ for the solid. As before, we performed the calculations for the temperatures $T^*=2.0$ and $T^*=3.0$. We have also run a number of simulations at several temperatures for the reference densities in order to compute the reference free energies of both phases in a wide range of temperatures. Then we selected a number of temperatures and ran several simulations at a series of densities for both phases. The values of pressure were used to fit the equations of state to second order polynomials and then we searched for the phase equilibrium.

B. High-temperature fluid-fluid equilibrium

At high temperature the fluid undergoes a weak first-order orientational transition from an isotropic to a nematic phase. In order to locate this transition, simulations in the isothermal-isobaric (NpT) ensemble were performed for different system sizes, pressures, and temperatures. For a given temperature, we first performed some preliminary short runs with a small system size to get rough estimates of the equilibrium densities and pressures; we then carried out longer simulations around the expected transition point for several values of the pressure and various system sizes. With these results, for each system size N we made use of the histogram reweighting techniques [19,34] to compute the value of the pressure $p_0(N,T)$ that maximizes volume fluctuations,

$$(\delta v)^2 = \langle v^2\rangle - \langle v\rangle^2, \tag{66}$$

where v denotes volume per particle. Let $v_0(N,T)$ and $\delta v_0(N,T)$ be the mean volume per particle and its fluctuation, respectively, at $p_0(N,T)$; if a first-order transition is present, then $\delta v_0(N,T)$ will have a finite nonzero value at the thermodynamic limit. Additionally, at the transition pressure $p_0(N,T)$ in this limit the volume distribution function becomes bimodal, with two narrow peaks centered at the v values of the coexisting phases.

The fulfillment of these trends can be assessed analyzing the cumulants of the volume distribution functions. We define the cumulant ratio by

$$G_4(N,T) = \frac{\langle (v-v_0)^4\rangle}{\langle (v-v_0)^2\rangle^2} \tag{67}$$

evaluated at $p=p_0(N,T)$. Then the presence of a first-order transition leads to $\lim_{N\to\infty}\delta v(N,T)>0$ and $\lim_{N\to\infty}G_4(N,T)$

=1. In contrast, in continuous transitions G_4 in the thermodynamic limit approaches a value different from unity which depends on the universality class to which the transition can be ascribed [35].

We chose $N=500$, 864, and 1372 particles for the reduced temperatures $T^*=2.0$ and $T^*=2.5$. At $T^*=3.0$ we have also considered a sample with $N=2048$ and finally for $T^*=3.5$ also systems with $N=2916$ and $N=4000$. Our results show that the transitions are weakly first order. Except at the highest temperature, the values of v_0 and δv_0 show only a small dependence (within the error bars) on system size, while the trends on the values of $G_4(N,T)$ confirm the first-order character of the transition. The values of the volumes per particle of the two coexisting phases can be evaluated as

$$v_\pm = v_0 \pm \delta v_0, \tag{68}$$

using the values of v_0 and δv_0 in the thermodynamic limit.

IV. RESULTS AND CONCLUSIONS

We have performed a series of Monte Carlo NpT runs with 500–4000 particle samples, with a thermalization stage of 25 000 trial steps and a production stage of 250 000 steps to evaluate the ensemble averages. In the NVT simulations for the thermodynamic integration, we have used 500 and 864 particle samples with 50 000 trial steps during equilibration and 100 000 steps in the production run. Every step in an N-particle sample implies N translation attempts and either N local updates of the particle orientation or a cluster move. Additionally, in NpT simulations a step also implies a volume change attempt.

In the integral equation calculations, pair functions are evaluated on uniform grids $r_j=j\Delta r$ and $k_j=j\Delta k$, $j=0,1,2,\ldots,N_r$, with $\Delta r\Delta k=\pi/N_r$; we set $\Delta r=0.01\sigma$ and $N_r=4096$. Series expansions in the orthogonal polynomials are truncated at $l_{\max}=m_{\max}=4$. We have checked the performance of the KYBG and TZLMBW equations, obtaining similar results for both closures. However, the TZLMBW equation leads to divergent transverse susceptibilities in the nematic phase at zero field for all approximate closures, including the mean spherical approximation. This feature, resulting from the presence of Goldstone modes in the ordered phase, is built into the TZLMBW equation, as was shown by Holovko and Sokolovska [36]. In contrast, the KYBG equation does not always reproduce the correct zero-field divergence in the transverse susceptibility of the ordered phases [9]. For this reason, we have focused here on the use of the TZLMBW relation, although preliminary comparisons of thermodynamic properties from both calculations indicate that the phase diagram will hardly be affected by the particular choice of the one-body equation. Note, however, that the divergence in the transverse susceptibility at zero field is associated with the existence of diverging correlations. As a consequence, it will not be possible to obtain converged solutions of the anisotropic Ornstein-Zernike equation at zero field in the nematic region using the standard numerical algorithms. We have implemented the procedure devised by Perera [37] to remove this zero-field singularity without really improving the situation. Fortunately, for small external fields the thermodynamic properties of the MS fluid depend quasilinearly on the field. Hence, we have obtained the zero-field results presented here using a simple extrapolation from calculations carried out at $W_0^*=1.0,0.8,0.6$. The validity of this approach was tested using the same procedure with simulation data; this showed that the extrapolated values differed from the zero-field simulation results by less than 0.1%.

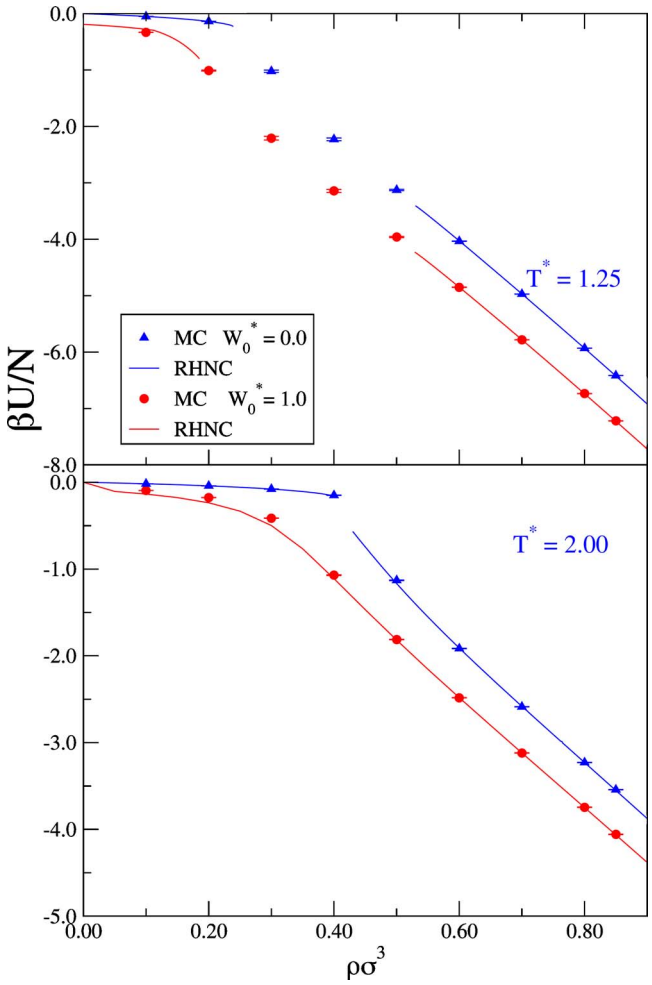

FIG. 1. (Color online) Integral equation and simulation results for the excess internal energy of the hard sphere Maier-Saupe fluid with and without external fields.

We can assess the quality of the anisotropic integral equation calculation so far as the thermodynamic properties are concerned from Figs. 1 and 2. Here we plot both the excess internal energy (Fig. 1) and the pressure (Fig. 2) calculated in the RHNC approximation, along with MC results. Optimization of the reference hard sphere diameter [28] somewhat improves the results at low temperatures, especially in the metastable region of the phase diagram, but is hardly noticeable when determining the gas-liquid equilibria. Since optimization implies a meaningful increase in the computational burden, we have restricted the calculation to the nonoptimized RHNC with $\sigma_{\mathrm{Ref}}=\sigma$. In any case, it is evident from the figures that the anisotropic RHNC closure is a reliable approximation for this type of system.

For calculations along an isotherm at a relatively high temperature ($T^*=3.5$, well above the gas-liquid equilibrium

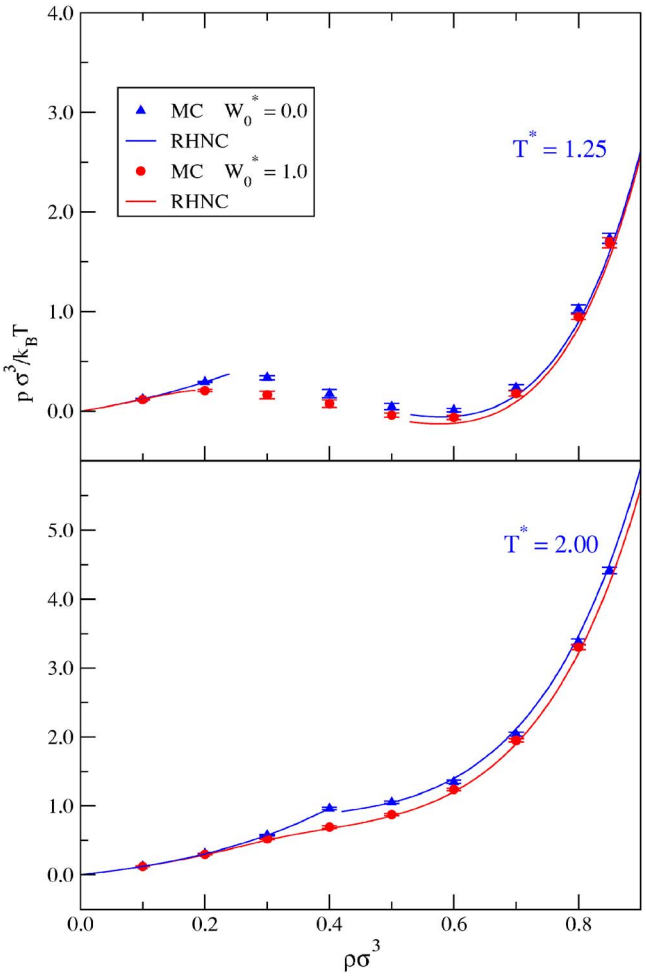

FIG. 2. (Color online) Integral equation and simulation results for the pressure of the hard sphere Maier-Saupe fluid with and without external fields.

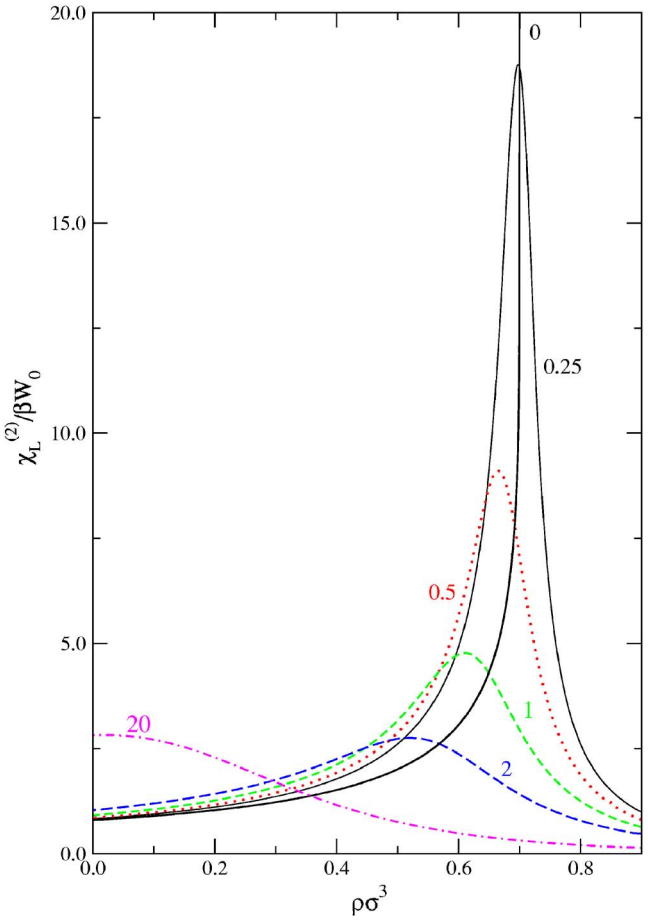

FIG. 3. (Color online) Density dependence of the two-particle component of the longitudinal susceptibility determined via the RHNC-TZLMBW equations at $T^*=3.5$ and various external fields W_0^*, as labeled.

curve), the two-particle component of the longitudinal susceptibility exhibits the characteristic divergence of an order-disorder transition as the external field vanishes (see Fig. 3). It is obvious from this result that we should expect an isotropic-nematic order-disorder transition to occur along the isotherm. If one now performs a series of NpT calculations at $T^*=3.8$ and pressures around $\beta p\sigma^3=6$, one finds the typical density histogram that occurs in the presence of a first-order phase transition, in consonance with our remarks in Sec. III B. This is illustrated in Fig. 4.

It is clear that we have to look for a first-order transition both in the high-temperature regime [(isotropic fluid)—(nematic fluid) transition] and in the low-temperature regime [(isotropic gas)—(nematic liquid) transition]. To that end, we solve the equilibrium conditions

$$\beta p(\rho_g\sigma^3,T^*)=\beta p(\rho_l\sigma^3,T^*), \tag{69}$$

$$\beta\mu(\rho_g\sigma^3,T^*)=\beta\mu(\rho_l\sigma^3,T^*), \tag{70}$$

using RHNC thermodynamics. The computed equilibrium curve is plotted in Fig. 5 together with the estimates obtained from our Monte Carlo calculations. As mentioned before, in the latter instance the equilibrium points for high temperatures ($T^*>2.0$) have been estimated from the NpT calculations. At lower temperatures, when the isotropic-nematic and the gas-liquid transitions are coupled, the thermodynamic integration method from NVT simulations is more reliable. At intermediate and high temperatures the two procedures yield identical results, within their statistical uncertainties. Data for the fluid-solid equilibrium obtained from thermodynamic integration are also shown in the figure. The first-order isotropic-nematic transition eventually meets the fluid-solid equilibrium, and one should expect to find again a first-order transition between isotropic and nematic solids. This is, in fact, what Zhang *et al.* [38] found for a simple cubic lattice, and since the interaction (3) induces no frustration effects the same results should be found in the most stable compact lattices (fcc or hcp). Now, since the isotropic-nematic first-order transition spans over all the temperature range, we do not have a proper gas-liquid critical point at which the difference between gas and liquid gets blurred. However, it is clear that around $T^*\approx 2.0$ there is a qualitative change in the behavior of the binodal curves. Actually, if one should introduce a small external field favoring nematic ordering a gas-liquid critical point would appear in the neighborhood of this temperature and $\rho\sigma^3\approx 0.5$. Increasing the external field, in

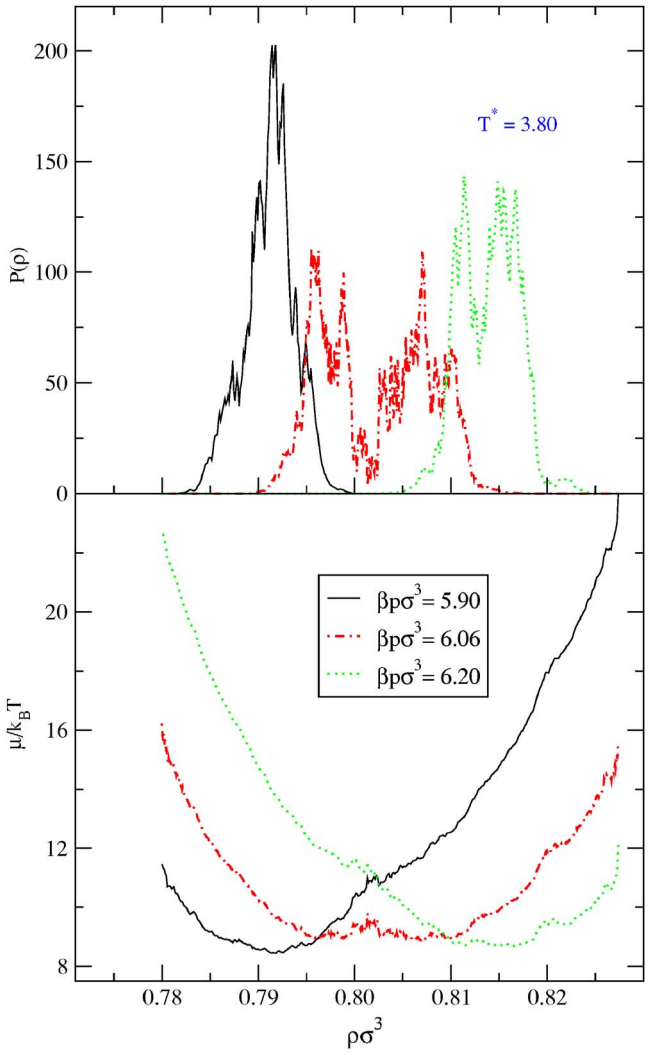

FIG. 4. (Color online) Density histograms (upper figure) and chemical potential distribution (lower figure) in *NpT* simulations of the Maier-Saupe fluid in the vicinity of the isotropic-nematic transition. The first-order equilibrium densities correspond to the two maxima (minima) of the density (chemical potential) histograms for the pressure at which the gas and liquid phase extrema reach equal values.

parallel to what happened in the Heisenberg spin fluid [9,11] or in the coplanar Maier-Saupe model [19], first should induce a decrease in the T_c^* due to a change in the universality class. This should be followed by a substantial increase of the critical temperature at moderate and high fields, due to the enhanced attractions induced by the nematic ordering. As a whole, the liquid phase is more stable in the presence of ordering fields.

Note that there is a region in which the gas side of the RHNC binodal lies above the RHNC nonsolution line (i.e., the line at which the solutions for the isotropic RHNC equation cease to exist). In this case we have estimated the binodal points by extrapolating the results obtained from the isotropic RHNC equation on the gas side to larger densities. This extrapolation procedure fails at temperatures above $T^*=2.5$ since the binodal starts to depart substantially from the RHNC spinodal. This shortcoming of the anisotropic RHNC

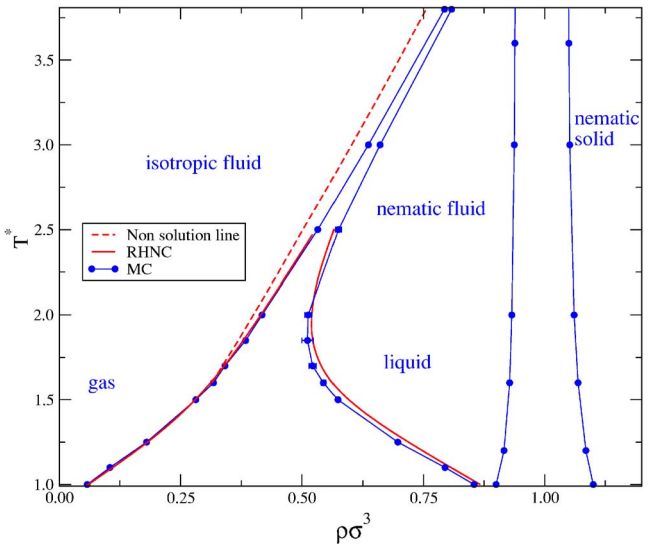

FIG. 5. (Color online) Phase diagram of the Maier-Saupe fluid determined from an anisotropic integral equation and computer simulation. The error bars at most simulation points have the same size as the symbols.

approach might be attributable to a certain degree of thermodynamic inconsistency or, more likely, to the failure of HNC-like approaches to capture the true criticality of fluids [39] because of the presence of complex solutions. Aside from this, the agreement between the RHNC coexistence curve and the simulation data is excellent. Both theory and simulation show that the hard sphere MS fluid exhibits a weak first-order isotropic-nematic transition at high temperatures that couples smoothly to a gas-liquid transition. This qualitatively agrees with the density functional theory predictions [17] and marks a clear difference with respect to the closely related Heisenberg spin fluid [9,10]. It is also interesting to see the effect that the change of dimensionality of the spatial distribution of the spins has on the critical behavior. Thus, one goes from a continuous BKT transition in the case of coplanar MS spins to a first-order transition when the particles are free to move in three dimensions in space. This is a well-known feature in lattice models [20] but it is nonetheless meaningful to see that in going from lattice to continuous models the same trends are manifest. Also, as in the case of the Heisenberg fluid, we observe here that the net attraction of the angle-dependent interactions is long ranged enough to bring about condensation, the only qualitative difference being that in the MS fluid the nature of the coupling between orientational and condensation transitions rules out the existence of tricritical or critical endpoints.

In summary, we have presented a detailed analysis of the phase behavior of hard sphere Maier-Saupe spin systems, with the aid of Monte Carlo computer simulations and an anisotropic Ornstein-Zernike integral equation. According to both theory and simulation this system undergoes a first-order isotropic-nematic transition continuously coupled to a gas-liquid transition. The theoretical approach has proven fairly accurate at moderate and low temperatures. The use of more sophisticated [40] closures at high temperatures might bypass the improper RHNC behavior at near critical conditions.

ACKNOWLEDGMENTS

The authors wish to thank Professor M.F. Holovko for his illuminating comments regarding the proper derivation of the transverse and longitudinal susceptibilities when dealing with nematic systems. E.L., N.G.A, and C.M. acknowledge support of the Dirección General de Investigación Científica y Técnica under Grant No. FIS2004-02954-C03-01 and the Dirección General de Universidades e Investigación of the Comunidad de Madrid under Grant No. S0505/ESP/0299-1.

[1] P. C. Hemmer and D. Imbro, Phys. Rev. A **16**, 380 (1977).
[2] M. J. P. Nijmeijer and J. J. Weis, Phys. Rev. Lett. **75**, 2887 (1995); **53**, 591 (1996).
[3] J. M. Tavares, M. M. Telo da Gama, P. I. C. Teixeira, J. J. Weis, and M. J. P. Nijmeijer, Phys. Rev. E **52**, 1915 (1995).
[4] F. Schinagl, H. Iro, and R. Folk, Eur. Phys. J. B **8**, 113 (1999); F. Schinagl, R. Folk, and H. Iro, J. Phys.: Condens. Matter **2**, 313 (1999).
[5] W. Fenz and R. Folk, Phys. Rev. E **67**, 021507 (2003).
[6] W. Fenz, R. Folk, I. M. Mryglod, and I. P. Omelyan, Phys. Rev. E **68**, 061510 (2003).
[7] T. G. Sokolovska, Physica A **253**, 459 (1998).
[8] F. Lado and E. Lomba, Phys. Rev. Lett. **80**, 3535 (1998).
[9] F. Lado, E. Lomba, and J. J. Weis, Phys. Rev. E **58**, 3478 (1998); **60**, 2429 (1999).
[10] E. Lomba, J. J. Weis, and C. F. Tejero, Phys. Rev. E **58**, 3426 (1998).
[11] T. G. Sokolovska and R. O. Sokolovskii, Phys. Rev. E **59**, R3819 (1999).
[12] I. P. Omelyan, I. M. Mryglod, R. Folk, and W. Fenz, Phys. Rev. E **69**, 061506 (2004).
[13] W. Fenz, I. P. Omelyan, and R. Folk, Phys. Rev. E **72**, 056121 (2005).
[14] I. P. Omelyan, W. Fenz, I. M. Mryglod, and R. Folk, Phys. Rev. E **72**, 031506 (2005).
[15] W. Maier and A. Saupe, Z. Naturforsch. A **14**, 882 (1959).
[16] G. R. Luckhurst and S. Romano, Proc. R. Soc. London, Ser. A **373**, 111 (1980); G. R. Luckhurst and P. Simpson, Mol. Phys. **47**, 251 (1982); G. R. Luckhurst, S. Romano, and P. Simpson, Chem. Phys. **73**, 337 (1982).
[17] M. M. Telo da Gama, Mol. Phys. **52**, 585 (1984); P. I. Teixeira and M. M. Telo da Gama, *ibid.* **86**, 1537 (1995).
[18] F. Lado, E. Lomba, and C. Martín, J. Mol. Liq. **112**, 51 (2004); **122**, 121 (2005).
[19] E. Lomba, C. Martín, N. G. Almarza, and F. Lado, Phys. Rev. E **71**, 046132 (2005).
[20] H. Kunz and G. Zumbach, Phys. Rev. B **46**, 662 (1992).
[21] V. L. Berezinskii, Sov. Phys. JETP **32**, 493 (1971); J. M. Kosterlitz and D. J. Thouless, J. Phys. C **6**, 1181 (1973).
[22] T. G. Sokolovska, M. F. Holovko, and R. O. Sokolovskii, Ukr. Fiz. Zh. **42**, 1304 (1997).
[23] J. P. Hansen and I. R. McDonald, *Theory of Simple Liquids* (Academic, London, 1986).
[24] D. Henderson, in *Fundamentals of Inhomogeneous Fluids*, edited by D. Henderson (Dekker, New York, 1992), Chap. 4.
[25] See, for example, G. Arfken, *Mathematical Methods for Physicists* (Academic, Orlando, 1985).
[26] F. Lado, Phys. Rev. A **8**, 2548 (1973).
[27] Y. Rosenfeld and N. W. Ashcroft, Phys. Rev. A **20**, 1208 (1979).
[28] F. Lado, Phys. Lett. **89**, 196 (1982).
[29] L. Verlet and J. J. Weis, Phys. Rev. A **5**, 939 (1972).
[30] D. Henderson and E. W. Grundke, J. Chem. Phys. **63**, 601 (1975).
[31] D. G. Triezenberg and R. Zwanzig, Phys. Rev. Lett. **28**, 1183 (1972); R. Lovett, C. Y. Mou, and F. P. Buff, J. Chem. Phys. **65**, 570 (1976); M. Wertheim, *ibid.* **65**, 2377 (1976).
[32] T. Morita and K. Hiroike, Prog. Theor. Phys. **23**, 1003 (1960).
[33] U. Wolff, Phys. Rev. Lett. **62**, 361 (1989).
[34] A. M. Ferrenberg and R. H. Swendsen, Phys. Rev. Lett. **63**, 1195 (1989).
[35] K. Binder, "*Introduction*" in *The Monte Carlo Method in Condensed Matter Physics*, 2nd ed., edited by K. Binder, Topics in Applied Physics, Vol. 71 (Springer-Verlag, Berlin, 1995).
[36] M. F. Holovko and T. Sokolovska, J. Mol. Liq. **82**, 161 (1999).
[37] A. Perera, Phys. Rev. E **60**, 2912 (1999).
[38] Z. Zhang, O. G. Mouritsen, and M. J. Zuckermann, Phys. Rev. Lett. **69**, 2803 (1992).
[39] E. Lomba, Mol. Phys. **68**, 87 (1989); E. Lomba and J. L. López Martín, J. Stat. Phys. **80**, 825 (1995), and references therein.
[40] G. Sarkisov and E. Lomba, J. Chem. Phys. **122**, 214504 (2005).